Wave-Driven Assembly of Quasiperiodic Patterns of Particles

Elena Cherkaev,[1] Fernando Guevara Vasquez,[1] China Mauck,[1] Milo Prisbrey,[2,*] and Bart Raeymaekers[2]
[1]Department of Mathematics, University of Utah, Salt Lake City, Utah 84112, USA
[2]Department of Mechanical Engineering, University of Utah, Salt Lake City, Utah 84112, USA

(Received 24 November 2020; accepted 5 March 2021; published 8 April 2021)

We theoretically show that a superposition of plane waves causes small (compared to the wavelength) particles dispersed in a fluid to assemble in quasiperiodic two or three-dimensional patterns. We experimentally demonstrate this theory by using ultrasound waves to assemble quasiperiodic patterns of carbon nanoparticles in water using an octagonal arrangement of ultrasound transducers, and we document good agreement between theory and experiments. The theory also applies to obtaining quasiperiodic patterns in other situations where particles move with linear waves, such as optical lattices.

DOI: 10.1103/PhysRevLett.126.145501

We demonstrate that a superposition (finite linear combination) of plane waves assembles quasiperiodic patterns of particles dispersed in a fluid, which is useful to fabricate quasicrystal-like structures [1–4] with feature size of approximately one wavelength. Experimental evidence of quasiperiodic patterns of particles or atoms obtained with specific fields, such as lasers [5–8] and ultrasound waves [9] exists. In contrast, we derive a general theory to obtain prescribed quasiperiodic symmetries [e.g., eightfold, tenfold in two dimensions (2D) and icosahedral in three dimensions (3D), among others], for any linear wavelike phenomenon. Quasicrystals can exhibit unusual physical properties, e.g., diamagnetic properties, or low electric conductivity that may be strongly dependent on the temperature, see, e.g., Refs. [4,10]. Quasicrystals also arise naturally in alloys (e.g., Ref. [11]) and when combining molecules (e.g., mycelles [12]). However, the specific symmetries are limited by the choice of metals or molecules, unlike in the theory we demonstrate in this Letter.

Quasicrystals are characterized by diffraction patterns with symmetries that do not correspond to any crystalline (periodic) materials, e.g., tenfold symmetry in 2D [13,14]. Mathematically they can be described by *quasiperiodic* functions via the "projection method," see, e.g., Refs. [14,15]. A function $f\colon \mathbb{R}^d \to \mathbb{R}$ is quasiperiodic if another function exists $g\colon \mathbb{R}^N \to \mathbb{R}$ with period $[0, 2\pi]^N$ and a matrix $\mathsf{K} \in \mathbb{R}^{d\times N}$ such that $d < N$, $f(\boldsymbol{x}) = g(\mathsf{K}^T\boldsymbol{x})$ and there are at most $d-1$ linearly independent vectors in range(K^T) with entries being integer multiples of 2π. Thus, f is a restriction of the N-dimensional function g to d dimensions (Appendix A, [16]).

Let $p(\boldsymbol{x})$ be a scalar field describing a time-harmonic wave phenomenon, e.g., the acoustic pressure in a fluid with dispersed spherical particles. We model the interaction between the waves and particles using an energy landscape or potential $\psi(\boldsymbol{x}) = U(p(\boldsymbol{x}), \nabla p(\boldsymbol{x}))$, whose minima correspond to locations where particles accumulate when subject to the field $p(\boldsymbol{x})$. This is a valid assumption for, e.g., optics [11,17,18] and ultrasound waves [19–25]. We show that if $p(\boldsymbol{x})$ is a quasiperiodic function, then its energy landscape and corresponding pattern of particles must also be quasiperiodic. Moreover, a quasiperiodic $p(\boldsymbol{x})$ can result from a superposition of plane waves. Experimental evidence supporting this observation exists in, e.g., optics, where five lasers (which can be modeled by plane waves) can create optical lattices with tenfold symmetries [5–8]. Thus, the objective of this Letter is to derive a general theory to assemble patterns of particles dispersed in a fluid, for any linear wave phenomenon. Further, we demonstrate the theory using 2D ultrasound wave fields, established with $2N$ ultrasound transducers, where N is the dimension of the higher dimensional space in the projection method [14,15]. We disperse 80 nm carbon nanoparticles in water and assemble them into quasiperiodic patterns with eightfold (octagonal) symmetry, using eight ultrasound transducers spatially arranged as a regular octagon. The theory is also valid in 3D, and is useful to conveniently fabricate materials with quasiperiodic patterns of particles embedded in a polymer matrix [22,23], such as those used in engineered composite materials and metamaterials, e.g., Ref. [26].

The pressure associated with an ultrasound wave is given by $\tilde{p}(\boldsymbol{x}, t) = \Re(p(\boldsymbol{x})\exp[-i\omega t])$, where $\Re$ is the real part of a complex number, $\boldsymbol{x} \in \mathbb{R}^d$, t is time, ω is the angular frequency, and $i = \sqrt{-1}$. The field p solves the Helmholtz equation $\Delta p + k^2 p = 0$, with wave number $k = \omega/c$ and wave propagation speed c. A small (relative to the wavelength λ) particle in a standing ultrasound wave is subject to the acoustic radiation force associated with that ultrasound wave [27–30]. Thus, at location $\boldsymbol{x}$ in an inviscid fluid, a small particle experiences a force $\boldsymbol{F}(\boldsymbol{x}) = -\nabla\psi(\boldsymbol{x})$, with ψ the acoustic radiation potential (ARP), given as

$$\psi(\boldsymbol{x}) = \mathfrak{a}|p(\boldsymbol{x})|^2 - \nabla p(\boldsymbol{x})^* \mathfrak{B} \nabla p(\boldsymbol{x}). \tag{1}$$

Here $\mathfrak{a} = \mathfrak{f}_1\kappa_0/4$, $\mathfrak{B} = 3\mathfrak{f}_2/(8\rho_0\omega^2)\mathsf{I}_d$, I_d is the $d \times d$ identity matrix, $\mathfrak{f}_1 = 1 - (\kappa_p/\kappa_0)$, $\mathfrak{f}_2 = 2(\rho_p - \rho_0)/(2\rho_p + \rho_0)$, and $*$ is the conjugate transpose. ρ and κ are the density and compressibility, with subscripts 0 and p referring to the fluid and particle, respectively. Particles assemble at the minima of the ARP because the acoustic radiation force approaches zero where the ARP is (locally) minimum, and points towards the minimum in its vicinity. We remark that this theory neglects interactions between particles, i.e., it relies only on primary (or direct) scattering. Furthermore, the same theory describes the optical pressure exerted on dielectric particles that are smaller than a wavelength, by taking $\mathfrak{B} = \mathbf{0}$, see, e.g., Refs. [17,18,31].

We consider the particular case where the wave field $p(\boldsymbol{x})$ is a superposition of plane waves given by

$$p(\boldsymbol{x};\boldsymbol{u}) = \sum_{j=1}^{N} \alpha_j \exp[i\boldsymbol{k}_j \cdot \boldsymbol{x}] + \beta_j \exp[-i\boldsymbol{k}_j \cdot \boldsymbol{x}]. \quad (2)$$

Here, $\boldsymbol{u} = [\alpha_1, \ldots, \alpha_N, \beta_1, \ldots, \beta_N]^T$ is a vector containing the nonzero complex amplitudes in Eq. (2) and $\boldsymbol{k}_j$ are the wave vectors with $|\boldsymbol{k}_j| = k$. We may obtain fields close to Eq. (2) by using N pairs of parallel-oriented ultrasound transducers with normal directions $\boldsymbol{k}_j$ as shown in Fig. 1 for $N = 4$ and $d = 2$. For each j, α_j, and β_j represent the amplitude and phase of the signals that drive a pair of parallel ultrasound transducers with normal $\boldsymbol{k}_j$, as indicated in Fig. 1. We refer to the vector $\boldsymbol{u}$ as "transducer operating parameters," although this ignores the acoustic and electric impedance that would more accurately model the ultrasound transducers. We leave the characterization of the quasiperiodic patterns of particles that can be achieved with the wave field Eq. (2) for future studies. However, when $N = d$ and the $\boldsymbol{k}_j$ are linearly independent in Eq. (2), the patterns of particles are periodic and are characterized in Ref. [32].

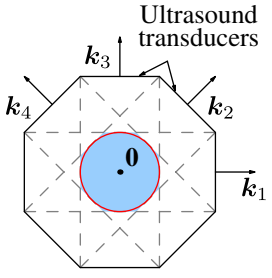

FIG. 1. Each parallel pair of ultrasound transducers establishes an ultrasound wave that is close to a plane wave in the rectangle delineated by the dotted lines perpendicular to the ultrasound transducers. The plane wave model Eq. (2) accurately represents the ultrasound wave field generated by this transducer arrangement in the blue region. The red circle indicates the region we evaluate.

The wave field Eq. (2) is a restriction to $\mathbb{R}^d$ of a wave field in $\mathbb{R}^N$ with period $[0, 2\pi]^N$. Thus, the wave field Eq. (2) can be made quasiperiodic. To show this, we define $p_N(\boldsymbol{y};\boldsymbol{u})$ using Eq. (2) with $\boldsymbol{y} \in \mathbb{R}^N$ and the canonical basis vectors $\boldsymbol{e}_j = (\delta_{ij})_{j=1}^N \in \mathbb{R}^N$ instead of the $\boldsymbol{k}_j$, $j = 1, \ldots, N$. Here, we use $\delta_{ij} = 1$ if $i = j$ and 0 otherwise. Clearly, $p_N(\boldsymbol{y};\boldsymbol{u})$ is periodic in $\boldsymbol{y}$ for any choice of complex amplitudes $\boldsymbol{u}$, and its period is the hypercube $[0, 2\pi]^N$. We use the convention that $\boldsymbol{x} \in \mathbb{R}^d$ and $\boldsymbol{y} \in \mathbb{R}^N$. A calculation (Appendix B, [16]) reveals that

$$p(\boldsymbol{x};\boldsymbol{u}) = p_N(\mathsf{K}^T\boldsymbol{x};\boldsymbol{u}), \quad (3)$$

where $\mathsf{K} = [\boldsymbol{k}_1, \ldots, \boldsymbol{k}_N] \in \mathbb{R}^{d\times N}$ determines whether the wave field is periodic or quasiperiodic. Naturally, the ARP ψ in $\mathbb{R}^d$ [see Eq. (1)] relates to a similar quantity ψ_N in $\mathbb{R}^N$ that is of the same form, but involves p_N instead of p and with identical $\mathfrak{a}$ but where the matrix $\mathfrak{B}_N = \mathsf{K}^T\mathfrak{B}\mathsf{K} \in \mathbb{R}^{N\times N}$ is different because of the chain rule (Appendix C, [16]), i.e.,

$$\psi(\boldsymbol{x};\boldsymbol{u}) = \psi_N(\mathsf{K}^T\boldsymbol{x};\boldsymbol{u}). \quad (4)$$

Hence, the ARP is quasiperiodic in $\boldsymbol{x}$ if $p(\boldsymbol{x};\boldsymbol{u})$ is quasiperiodic in $\boldsymbol{x}$.

The superposition of plane waves [Eq. (2)] predicts 2D quasiperiodic patterns of particles with prescribed symmetries. In the particular case of 80 nm carbon nanoparticles dispersed in water, we use $c_0 = 1500$ m/s, $c_p = 5300$ m/s, $\rho_0 = 1000$ kg/m^3, and $\rho_p = 2100$ kg/m^3. Since $\kappa = 1/(\rho c^2)$, we obtain $\mathfrak{a} \approx 5.7424 \times 10^6$ and $\mathfrak{B} \approx (0.2115)\mathsf{I}_2$ in Eq. (1). We intend the patterns of particles within the octagonal arrangement of ultrasound transducers in Fig. 1 to show eightfold symmetry. Figure 2 illustrates simulations of different symmetries for the carbon nanoparticles in water in the far field, i.e., the ultrasound transducers are sufficiently far

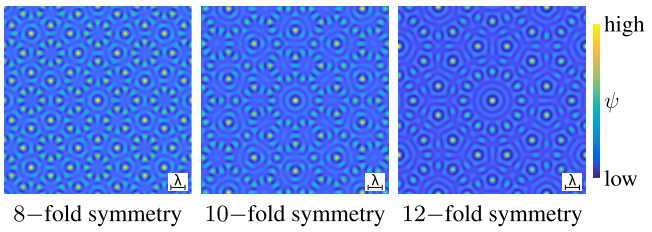

FIG. 2. Examples of the ARP that lead to quasiperiodic 2D patterns of particles. The wave vectors are $\boldsymbol{k}_j = [\cos\theta_j, \sin\theta_j]^T$, where $\theta_j = j\pi/N$, $j = 0, \ldots, N-1$ and $2N \in \{8, 10, 12\}$ corresponds to the desired order of rotational symmetry, i.e., eight-, ten-, or twelvefold symmetry. The ultrasound transducer operating parameters in Eq. (2) are $\boldsymbol{u} = [1, \ldots, 1]^T \in \mathbb{R}^{2N}$. The computation was performed using a uniform grid of the square $[-7\lambda, 7\lambda]^2$ with 1024^2 points. The color scale shows arbitrary units.

from the region that we display. For instance, if we drive the eight ultrasound transducers in Fig. 1 with the same amplitude and phase, i.e., $\boldsymbol{u} = [1, \ldots, 1]^T \in \mathbb{R}^8$, we obtain patterns of particles with an eightfold symmetry and center of rotation at the origin (the center of the red circle in Fig. 1). Figure 2 also shows quasiperiodic patterns of particles with tenfold and twelvefold symmetries that can be obtained by arranging the ultrasound transducers in Fig. 1 as either a regular decagon or dodecagon, instead of an octagon. Thus, we obtain known quasiperiodic symmetries in 2D, e.g., the tenfold symmetry is the same symmetry encountered in Penrose tilings [2,13,14]. We also point out that ultrasound transducer arrangements other than regular polygons are possible and will yield patterns of particles with other symmetries.

We used the setup of Fig. 3 to experimentally obtain quasiperiodic patterns with eightfold symmetries. The setup comprises a polycarbonate octagonal reservoir with water, 80 nm carbon nanoparticles, and sodium dodecyl benzene sulfonate (NaDDBS) surfactant [33]. The reservoir is lined with eight ultrasound transducers along its perimeter (SM111 piezoelectric material, with center frequency of 1 MHz), driven by a function generator. The distance between two parallel ultrasound transducers is 5 cm and each ultrasound transducer is 2 cm wide (or $40\lambda/3$). The depth of the liquid is approximately 1 cm (or 7λ, when $c_0 = 1500$ m/s). Thus, boundary effects from the reservoir and the free liquid surface are negligible and the theory and experiments only consider bulk ultrasound waves. Brownian motion of the particles is negligible in the experiments (Appendix D, [16]).

We compare simulations of the ARP obtained from the theoretical plane wave superposition Eq. (2), where particles assemble at the minima of the ARP, to experimentally obtained patterns of particles, for two specific experiments. In experiment 1, we impose ultrasound transducer operating parameters $\boldsymbol{u} = [1, 1, 1, 1, 1, 1, 1, 1]^T$ and in experiment 2 we impose $\boldsymbol{u} = [1, -1, 1, 1, 1, -1, 1, 1]^T$. Figure 4 shows the simulated ARP in the region $[-7\lambda, 7\lambda]^2$, and we indicate the region we evaluate as a red circle, as in Fig. 1. We used explicit expressions for the gradient and Hessian of the ARP to predict the locations where particles assemble, by identifying points where the Hessian is sufficiently positive definite (minimum eigenvalue greater than 10^{-6}) and the gradient is sufficiently small (less than 4×10^{11}). We show the simulated locations where particles assemble in red, superimposed on the experimental results (photographs, where dark areas show columns of particles viewed from the top, as in Ref. [23]). We manually register the simulated and experimental results with MATLAB's FITGEOTRANS at the points indicated by "+" signs in Fig. 4, assuming a 2D projective transformation. Finally, we qualitatively compare the simulated and experimental results by superimposing the simulated locations where we predict particles assemble (red) and experimentally obtained patterns of particles (blue), and we mark the overlapping locations (blue and red) in black. We observe good qualitative agreement between simulations and experiments.

We quantified the agreement between simulations and experiments within the red circle of diameter $D = 40\lambda/3$ as follows. We binarized the photographs of the experimental results, using MATLAB's IMBINARIZE with sensitivity 0.45.

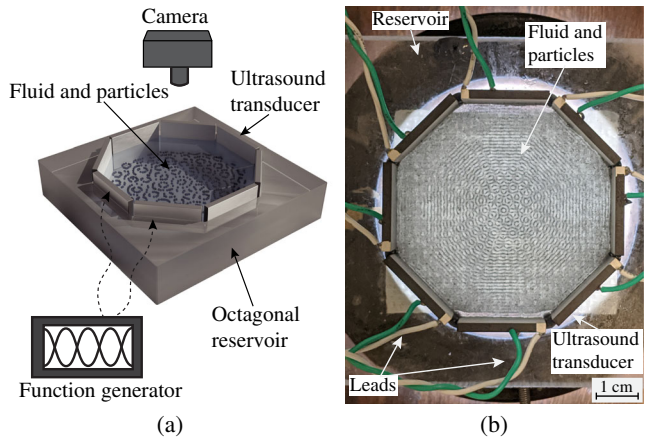

FIG. 3. (a) Schematic of the experimental setup showing its components and (b) photograph of the experimental setup (top view) showing a typical experiment with 80 nm carbon nanoparticles in water.

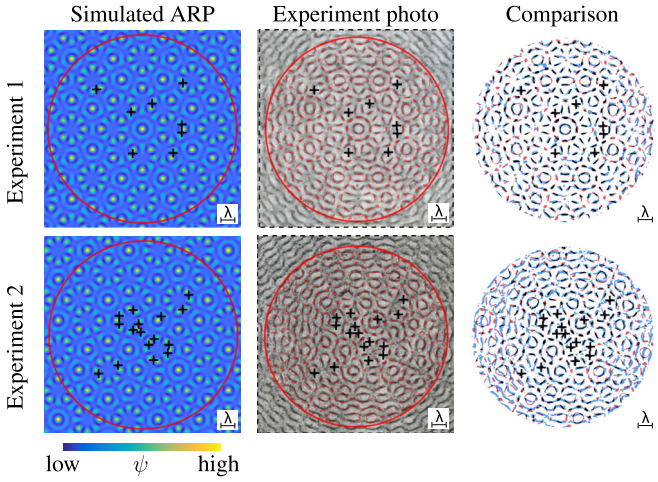

FIG. 4. Simulated ARP (first column, particles assemble at minima) and experimentally obtained patterns of particles with the minima of the simulated ARP superimposed in red (second column), for experiments 1 and 2, showing distinct quasiperiodic patterns with eightfold symmetries. We superimpose the simulated ARP minima where we predict particles assemble (red) and experimentally obtained patterns of particles (blue) (third column). We mark the overlapping locations (blue and red) in black. Each image shows a red circle where we expect good agreement with the plane wave model (see also Fig. 1) and "+" signs indicate the registration between the simulated ARP and the experimental results.

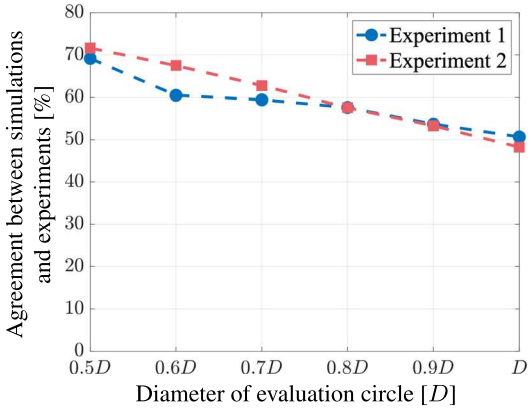

FIG. 5. Agreement between simulations and experiments as a function of evaluation circle diameter $D = 40\lambda/3$.

We determined the fraction of the total area of the simulated clusters that is inside the experimentally determined clusters, i.e., the black area divided by the sum of the black and blue areas using the color convention in the comparison column of Fig. 4. Figure 5 shows that the agreement between simulations and experiments improves with decreasing size of the evaluation circle with diameter αD, with $\alpha \in [1/2, 1]$. In Fig. 5, the fraction of agreement between simulations and experiments increases linearly with decreasing size of the evaluation circle. Thus, the simulations and experiments agree most closely at the origin, which is consistent with Eq. (2) being a far-field model. Other sources of error in the model Eq. (2) include neglecting the boundary reflections and the finite width of the ultrasound transducers.

We have shown that linear wave phenomena can assemble quasiperiodic patterns of particles. Since linear wave phenomena are common in physics, our findings apply to a broad variety of different physical situations, including ultrasound waves, electromagnetic waves, elastic waves, amongst others. We illustrated this principle theoretically with plane waves in a fluid, and demonstrated it experimentally by assembling 80 nm carbon nanoparticles dispersed in water into patterns with eightfold symmetries, using ultrasound waves. The theory accurately predicts the experimental patterns of particles. Thus, this theory and experimental demonstration provides a pathway upon which to base a manufacturing platform for quasicrystal-like structures of inclusions in a polymer matrix. Such materials could help with the experimental study of the physical properties of quasicrystals. These quasiperiodic materials could have different mechanical or electrical properties than a material with a random arrangement of particles.

F. G. V., C. M., M. P., and B. R. acknowledge support from the Army Research Office under Contract No. W911NF-16-1-0457. All authors contributed to writing the manuscript. The mathematical theory and results were derived by E. C., F. G. V., and C. M. The simulations were designed and performed by F. G. V., C. M., M. P., and B. R. using MATLAB. The experiments were designed by all authors and implemented and performed by M. P. and B. R. E. C. acknowledges partial support from the National Science Foundation Grant No. DMS-1715680.

*Present address: Acoustics and sensors team, Materials Physics and Applications Group (MPA-11), Los Alamos National Laboratory, Los Alamos, NM 87545, USA.

[1] D. Shechtman, I. Blech, D. Gratias, and J. W. Cahn, Metallic Phase with Long-Range Orientational Order and No Translational Symmetry, Phys. Rev. Lett. **53**, 1951 (1984).
[2] A. Yamamoto, Crystallography of quasiperiodic crystals, Acta Crystallogr. Sect. A **52**, 509 (1996).
[3] C. Janot, *Quasicrystals* (Clarendon Press, Oxford University Press, Oxford, 2012).
[4] Z. M. Stadnik, *Physical Properties of Quasicrystals* (Springer Science & Business Media, New York, 1999), Vol. 126.
[5] Y. Roichman and D. G. Grier, Holographic assembly of quasicrystalline photonic heterostructures, Opt. Express **13**, 5434 (2005).
[6] X. Wang, J. Xu, J. C. W. Lee, Y. K. Pang, W. Y. Tam, C. T. Chan, and P. Sheng, Realization of optical periodic quasicrystals using holographic lithography, Appl. Phys. Lett. **88**, 051901 (2006).
[7] J. Mikhael, J. Roth, L. Helden, and C. Bechinger, Archimedean-like tiling on decagonal quasicrystalline surfaces, Nature (London) **454**, 501 (2008).
[8] X. Sun, Y. Wu, W. Liu, W. Liu, J. Han, and L. Jiang, Fabrication of ten-fold photonic quasicrystalline structures, AIP Adv. **5**, 057108 (2015).
[9] F. M. de Espinosa, M. Torres, G. Pastor, M. A. Muriel, and A. L. Mackay, Acoustic quasi-crystals, Europhys. Lett. **21**, 915 (1993).
[10] E. M. Barber, Chemical bonding and physical properties in quasicrystals and their related approximant phases: Known facts and current perspectives, Appl. Sci. **9**, 2132 (2019).
[11] A. Ashkin and J. Dziedzic, Optical trapping and manipulation of viruses and bacteria, Science **235**, 1517 (1987).
[12] C. R. Iacovella, A. S. Keys, and S. C. Glotzer, Self-assembly of soft-matter quasicrystals and their approximants, Proc. Natl. Acad. Sci. U.S.A. **108**, 20935 (2011).
[13] R. Penrose, Pentaplexity: A class of nonperiodic tilings of the plane, Math. Intelligencer **2**, 32 (1979).
[14] N. de Bruijn, Algebraic theory of Penrose's non-periodic tilings of the plane, Indagat. Math **84**, 39 (1981).
[15] M. Duneau and A. Katz, Quasiperiodic Patterns, Phys. Rev. Lett. **54**, 2688 (1985).
[16] See Supplemental Material at http://link.aps.org/supplemental/10.1103/PhysRevLett.126.145501 for Appendices A–D.
[17] K. C. Neuman and S. M. Block, Optical trapping, Rev. Sci. Instrum. **75**, 2787 (2004).
[18] T. A. Nieminen, G. Knöner, N. R. Heckenberg, and H. Rubinsztein-Dunlop, Physics of optical tweezers, Methods Cell Biol. **82**, 207 (2007).

[19] J. Friend and L. Y. Yeo, Microscale acoustofluidics: Microfluidics driven via acoustics and ultrasonics, Rev. Mod. Phys. **83**, 647 (2011).
[20] M. Wiklund, S. Radel, and J. J. Hawkes, Acoustofluidics 21: Ultrasound-enhanced immunoassays and particle sensors, Lab Chip **13**, 25 (2013).
[21] C. R. P. Courtney, C. E. M. Demore, H. Wu, A. Grinenko, P. D. Wilcox, S. Cochran, and B. W. Drinkwater, Independent trapping and manipulation of microparticles using dexterous acoustic tweezers, Appl. Phys. Lett. **104**, 154103 (2014).
[22] J. Greenhall, F. Guevara Vasquez, and B. Raeymaekers, Ultrasound directed self-assembly of user-specified patterns of nanoparticles dispersed in a fluid medium, Appl. Phys. Lett. **108**, 103103 (2016).
[23] M. Prisbrey, J. Greenhall, F. Guevara Vasquez, and B. Raeymaekers, Ultrasound directed self-assembly of three-dimensional user-specified patterns of particles in a fluid medium, J. Appl. Phys. **121**, 014302 (2017).
[24] L. Meng, F. Cai, F. Li, W. Zhou, L. Niu, and H. Zheng, Acoustic tweezers, J. Phys. D **52**, 273001 (2019).
[25] A. Marzo and B. W. Drinkwater, Holographic acoustic tweezers, Proc. Natl. Acad. Sci. U.S.A. **116**, 84 (2019).
[26] S. J. Corbitt, M. Francoeur, and B. Raeymaekers, Implementation of optical dielectric metamaterials: A review, J. Quantum Spectrosc. Radiat. Transfer **158**, 3 (2015).
[27] L. P. Gor'kov, On the forces acting on a small particle in an acoustical field in an ideal fluid, Dok. Akad. Nauk SSSR **140**, 88 (1961) [Dokl. Phys. **6**, 773 (1961)], http://mi.mathnet.ru/eng/dan25473.
[28] L. V. King, On the acoustic radiation pressure on spheres, Proc. R. Soc. A **147**, 212 (1934).
[29] H. Bruus, Acoustofluidics 7: The acoustic radiation force on small particles, Lab Chip **12**, 1014 (2012).
[30] M. Settnes and H. Bruus, Forces acting on a small particle in an acoustical field in a viscous fluid, Phys. Rev. E **85**, 016327 (2012).
[31] J.-L. Thomas, R. Marchiano, and D. Baresch, Acoustical and optical radiation pressure and the development of single beam acoustical tweezers, J. Quant. Spectrosc. Radiat. Transfer **195**, 55 (2017).
[32] F. Guevara Vasquez and C. Mauck, Periodic particle arrangements using standing acoustic waves, Proc. R. Soc. A **475**, 20190574 (2019).
[33] M. F. Islam, E. Rojas, D. M. Bergey, A. T. Johnson, and A. G. Yodh, High weight fraction surfactant solubilization of single-wall carbon nanotubes in water, Nano Lett. **3**, 269 (2003).